# Supporting Information

# Isolation and in vitro culture of rare cancer stem cells from patient-derived xenografts of pancreatic ductal adenocarcinoma

Philip C. Gach,[1] Peter J. Attayek,[2] Gabriela Herrera,[3] Jen Jen Yeh,[3,4,5] and Nancy L. Allbritton[1,2,3,5]*

[1]*Department of Chemistry, University of North Carolina, Chapel Hill, North Carolina 27599*

[2]*Department of Biomedical Engineering, University of North Carolina, Chapel Hill, North Carolina 27599 and North Carolina State University, Raleigh, North Carolina 27695*

[3]*Lineberger Comprehensive Cancer Center, University of North Carolina, Chapel Hill, North Carolina 27599*

[4]*Department of Surgery, Division of surgical Oncology, University of North Carolina, Chapel Hill, North Carolina 27599*

[5]*Department of Pharmacology, University of North Carolina, Chapel Hill, North Carolina 27599*

* Corresponding author

E-mail: nlallbri@unc.edu. Fax: 919-962-2388, Phone: 919-966-2291

## EXPERIMENTAL SECTION

**Reagents.** The following materials were obtained from the Aldrich Chemical Company (St. Louis, MO): iron(III) chloride tetrahydrate, iron(III) chloride anhydrous, iron(III) nitrate nonahydrate, toluene (reagent grade), triarylsulfonium hexafluorophosphate salts, mixed, 50% in propylene carbonate, γ-butyralactone (GBL, 99+%), 1-methoxy-2-propanol (SU8 developer, 98.5%). EPON resin 1002F (phenol, 4,4'-(1-methylethylidene)bis-, polymer with 2,2'-[(1-methylethylidene) bis(4,1-phenyleneoxymethylene]bis-[oxirane]) was obtained from Miller-Stephenson (Sylmar, CA) and (heptadecafluoro-1,1,2,2-tetrahydrodecyl)trichlorosilane was purchased from Gelest Inc (Morrisville, PA). Dulbecco's modified Eagle's medium (DMEM), fetal bovine serum (FBS), 1X phosphate buffered saline (PBS), pH 7.4, 0.05% trypsin with EDTA solution and penicillin/streptomycin were received from Invitrogen (Carlsbad, CA). Sylgard 184 silicone elastomer kit (PDMS) was received from Dow Corning (Midland, MI). Fibronectin extracted and purified from human plasma was obtained from Chemicon International Inc. (Temecula, CA). A Quantum FITC-5 MESF kit was obtained from Bangs Laboratories, Inc. (Fishers, IN). Wild-type HeLa cells were purchased from the American Type Culture Collection (ATCC, Manassas, VA). All other chemicals were procured from Fisher Scientific (Pittsburgh, PA).

**Fabrication of micropallet arrays and PDMS chambers.** Magnetic 1002F photoresist (61% EPON resin 1002F, 32.65% gamma-butyrolactone, 6.1% triarylsulfonium hexafluoroantimonate salts and 0.25% oleic acid functionalized $\gamma Fe_2O_3$ nanoparticles by weight percentage) was synthesized as described previously.[1] The magnetic photoresist was then spin-coated to a 75 μm thick film on a glass slide (B270 150mm diam. x 0.9mm thick, Valley Design Corp., Santa Cruz, CA). Prior to photoresist application, glass slides were cleaned with acetone,

isopropyl alcohol, deionized water and treated in a plasma cleaner for 20 min (Harrick Plasma, Ithaca, NY). Coated slides were covered with foil and allowed to soft bake in a 95$^{o}$C convection oven (Isotemp Oven, Fisher Scientific, Pittsburgh, PA) for 1 h. After the slides cooled, the film was exposed to UV light (Karl Suss MA6/BA6, SUSS MicroTech, Garching, Germany) through a chrome mask. Slides were post baked at 95$^{o}$C for a 10 min and then cooled to room temperature. Film areas not exposed to UV light were then removed by incubation in SU-8 developer for 10 min. Arrays were rinsed briefly with fresh SU-8 developer and isopropyl alcohol. Following solvent removal with a stream of nitrogen gas, the arrays were hard baked on a 120$^{o}$C hot plate for 1 h (825-HP, VWR, West Chester, PA). Large arrays were composed of a 1350 x 950 array of micropallets with dimensions of 50 × 50 × 75 μm (L × W × H) and a 25 μm gap between micropallets. Every 50$^{th}$ and 51$^{st}$ micropallet was replaced with a 125 × 125 μm square element with 50 μm embedded numbers to assist in identifying micropallet coordinates. This generated an array with a total size of 101.225 × 71.250 mm consisting of 1,280,448 micropallets and 513 numbered micropallets.

Following pallet fabrication, a plastic cassette was glued around the pallet array with PDMS. The 105 × 75 × 6 mm culture chamber was machined from 3 mm ABS filament (MakerBot Industries, Brooklyn, NY) with a BFB 3000 plus 3D printer (3D systems, Rock Hill, SC). A small side chamber was included on the culture chamber to allow removal of air bubbles from the micropallet array chamber when cells were cultured. The array was coated with hydrophobic perfluoroalkylsilane layer ((heptadecafluoro-1,1,2,2-tetrahydrodecyl)trichloro-silane) by chemical vapor deposition as described previously.[2] The arrays were sterilized by rinsing with 95% ethanol and dried in a tissue culture hood. Excess ethanol was removed with five PBS rinses. The top surfaces of the micropallets on the array were then coated with 5 mL of

25 μg/mL fibronectin in PBS for one hour at room temperature. Following surface coating, the array was rinsed 5 times with PBS.

**Conditioned media.** Conditioned media was developed by growing subconfluent cultures of cells in DMEM supplemented with FBS (10%), L-glutamine (584 mg $L^{-1}$), penicillin (100 units $mL^{-1}$) and streptomycin (100 μg $ml^{-1}$) for 48 h. Conditioned media for tumor spheroid formation lacked FBS. Media collected from GFP-HeLa, Panc-1 or pancreatic xenograft cell cultures was employed as conditioned media for colony expansion of their respective cells. The supernatant was centrifuged (3,000 g, 20 min), stored at -20$^{o}$C and thawed immediately prior to use.

**Image processing and analysis.** Raw images were saved to the computer hard drive and the data processed and segmented by a custom MATLAB program. First the images were processed with a combination of adaptive wiener filtering, top hat filtering and/or modified top hat filtering to correct for uneven illumination and autofluorescence of the micropallets.[3] The image processing procedure that produced the greatest increase in signal to noise ratio (S/N) was determined. The processed images were then segmented using a user-defined or automated thresholding approach. The threshold value was determined for each image to maximize the detection of true positives. Size exclusion filters were then employed to eliminate artifacts larger or smaller than a user-defined maximum and minimum diameter respectively. Finally, negative control fluorescence images were utilized to remove remaining artifacts from the fluorescence image of the target cell. The resulting cell coordinates were then manually imaged to confirm cellular identification.

**Micropallet release and collection.** Select micropallets were released from the array as described previously.[4] Dislodged micropallets were magnetically attracted onto a collection substrate as described previously.[1] Following identification of target cells, the glass cover was

replaced with a multiwell collection substrate. The collection substrate consisted of a 100 × 70 array of 1 × 1 mm PDMS wells 100 μm in depth fabricated as described previously.[5] A plastic cassette was attached to the multiwell plate using PDMS as a glue. The 103 × 73 × 2 mm cassette was manufactured from 3mm ABS filament (MakerBot Industries, Brooklyn, NY) with a BFB 3000 plus 3D printer (3D systems, Rock Hill, SC). The cassette was autoclaved, rinsed with ethanol and allowed to air dry in a tissue culture hood. The chamber was then incubated with 25 μg/mL fibronectin in 1X PBS for 2 hrs. Prior to use, the wells were rinsed ×5 with 1X PBS. The collection cassette was then mated to the micropallet cassette so that 1X PBS filled the space between the arrays. The array was then transferred to a Nikon Eclipse TE300 inverted microscope (Nikon Instruments Inc., Melville, NY) and micropallets holding target cells were released. Detached micropallets were collected by applying a magnetic field using a 1.27 cm diam. × 2.54 cm thick axially magnetized neodymium magnet (K&J Magnetics, Inc., Jamison, PA).[1] Following collection of all target micropallets, the small magnet was replaced by a 10.16 × 10.16 × 1.27 cm (L × W × H) neodymium magnet (K&J Magnetics, Inc., Jamison, PA) and transferred to a sterile hood. The magnet was held in contact with the collection plate during removal of the cassette and replacement of the 1X PBS with conditioned media. The magnet was then removed and the collection plate moved to an incubator for culture of isolated cells.

## RESULTS

### Image acquisition.

*Imaging criteria*. Minimizing array screening time was desired to reduce experimental times and diminish cell exposure to room temperatures and atmospheric $CO_2$ levels.[6] Array imaging times were dominated by the time for image acquisition and stage movement. Further,

image processing will only be effective if the raw captured images are of sufficient quality. Analysis of fluorescence images demands that cellular fluorescence be significantly brighter than the background signal (high S/N). Exposure of cells to the illumination light should be minimal to reduce imaging time along with photobleaching[7] and phototoxicity.[8] Another consideration of image acquisition is resolution since the number of pixels/cell must be sufficient to reduce the impact of camera noise.

*Microscopy considerations.* An automated wide-field epifluoresence imaging system was designed to meet the above requirements for efficient screening of large micropallet arrays. An Olympus MVX10 MacroView microscope offered a large field of view with microscope objectives (0.63X – 2.0X) of high numerical apertures (NA) ranging from 0.15 to 0.50. Additionally, the microscope body possessed a variable zoom selection that expanded the total magnification of the microscope from 0.4X to 12.6X. A high NA objective was crucial to efficiently collecting the fluorescence signal since the light gathering power of an objective for epi-illumination ($F_{epi}$) is governed by the equation:

$$F_{epi} = 10^4 \times NA_{obj}^4 / M^2$$

where M is the magnification and $NA_{obj}$ is the NA of the objective. The MVX10 1X objective (NA 0.25) provided 1526 × greater $F_{epi}$ than a standard Nikon Plan UW 1X objective (NA 0.04). The Hamamatsu ORCA-Flash4.0 camera was utilized because it offered excellent sensitivity (>50% quantum efficiency from 450 – 750 nm), low noise (1.3 e- at 100 frames/s), high-speed (100 frames/s) and a large field of view and high resolution (4.0M pixels at 6.5 μm x 6.5 μm each). The combined system offered a large field of view ranging from 1,225 $mm^2$ to 1.17 $mm^2$ with excellent light collection (Table S1). This imaging system generated pixel sizes of 17.10 μm

– 0.53 μm as the field of view changed from 1,225 $mm^2$ to 1.17 $mm^2$, respectively.

| Effects of microscope objective on imaging parameters | | | | | |
|---|---|---|---|---|---|
| Objective/Mag | Pixel Size (μm) | Field of View ($mm^2$) | Images per Array[a] | Imaging Time (min)[ab] | Sensitivity[c] |
| 0.63X / 0.63 | 17.10 | 1225.88 | 7 | 0.27 | — |
| 0.63X / 2.00 | 5.27 | 116.46 | 67 | 1.73 | 0.778 ± 0.036 |
| 0.63X / 6.30 | 1.68 | 11.79 | 657 | 13.65 | 0.993 ± 0.007 |
| 1X / 0.63 | 10.64 | 475.25 | 17 | 0.55 | — |
| 1X / 2.00 | 3.34 | 46.74 | 166 | 3.85 | 1.000 ± 0.000 |
| 1X / 6.30 | 1.05 | 4.60 | 1685 | 32.94 | 1.000 ± 0.000 |
| 2X / 0.63 | 5.40 | 122.32 | 64 | 1.67 | 0.984 ± 0.016 |
| 2X / 2.00 | 1.68 | 11.84 | 654 | 13.58 | 1.000 ± 0.000 |
| 2X / 6.30 | 0.53 | 1.17 | 6616 | 120.66 | 1.000 ± 0.000 |
| [a] Image number and time from screening of a 10.1 x 7.1 cm array [b] All images taken at 200 ms exposure | | | | | |
| [c]Sensitivity determined using fluorescein-labled microspheres (7-9 μm diameter) | | | | | |

**Table S1**. Effects of MVX-10 microscope objective on imaging parameters. Accurate sensitivity values could not be determined for magnifications below which allowed manual analysis.

*Objective/Magnification selection.* Imaging a 10.1 cm × 7.1 cm micropallet array was automated using a custom MATLAB program (Figure S1). During optimization of image acquisition, the light exposure time was fixed at 200 ms and the final magnification set using both the objective and a variable magnification zoom within the microscope. Complete imaging of the array with this system required between 0.27 and 121 min. as the total magnification changed from 0.4X to 12.6X, respectively (Table S1). A microscope objective and magnification were chosen in succeeding experiments which provided 100% sensitivity and minimal array imaging time. Detection sensitivity was assessed by comparing images microspheres (7-9 μm diameter) labeled with molecules of equivalent soluble fluorochrome (MESF) units of fluorescein by manual screening and the 'Kapur Entropy' automated threshold algorithm. The 1X objective paired with a 2X magnification achieved 100% sensitivity and required a short duration for imaging of the 10.1 cm × 7.1 cm micropallet array (3 min 51 s). Additionally, the small pixel size

(3.34 µm/pixel) provided multiple pixels per cell which aided cellular analysis and removal of bright background pixels as described in the "Imaging Analysis" section.

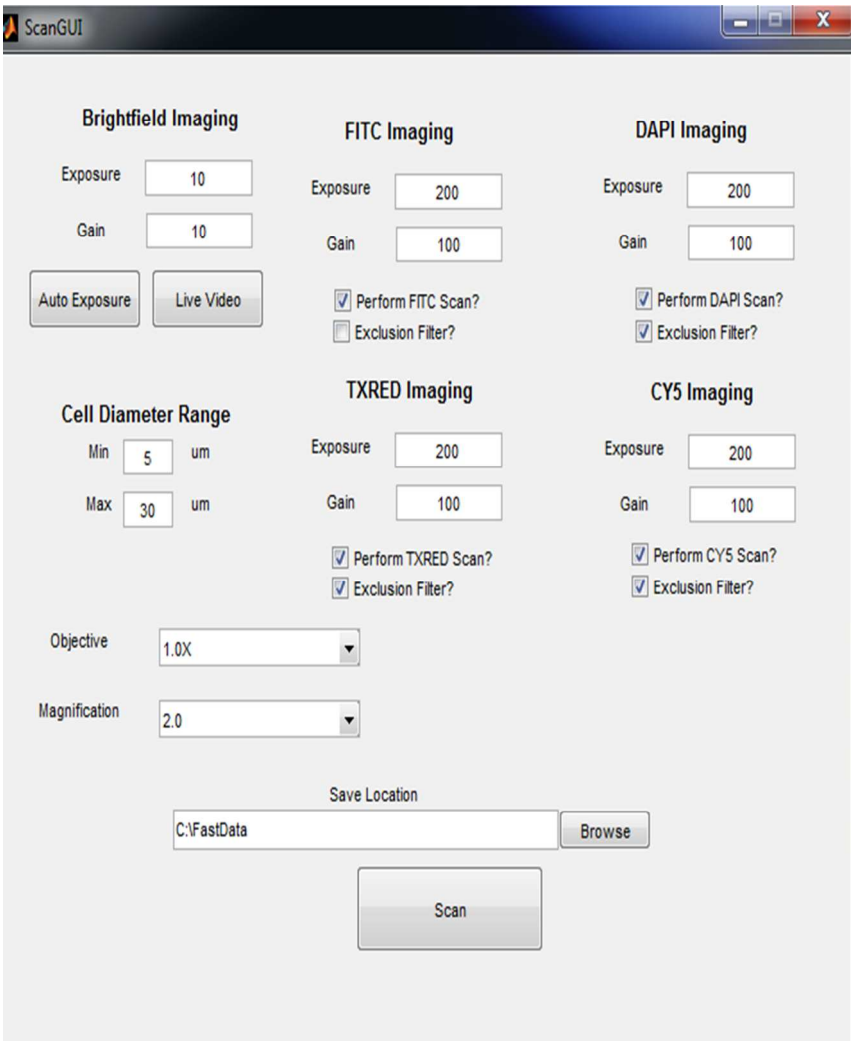


**Figure S1**. Image acquisition GUI for large array screening. Front panel of the GUI designed for user input to controlling array imaging. The ScanArray GUI includes features for controlling brightfield exposure, picking of fluorescence imaging filter sets and exposures, objective and magnification choice, selection of size filter and data save location.

**Image processing.**

*Fluorescence exposure optimization.* A micropallet array was loaded with a 1:10 mixture of GFP-HeLa cells to HeLa cells and green fluorescent images were acquired of the array. Strategies for improving the quality of images prior to analysis were evaluated by measuring the S/N of the GFP-HeLa cells. The signal (S) was defined as the mean intensity of the GFP-HeLa cells while the noise (N) was defined as the standard deviation of the background intensity. S/N was maximized by optimizing the camera exposure duration as shown in Figure S2. Optimal exposure times were selected as the duration in which increasing the time no longer increased S/N.The plot of S/N *vs* exposure duration for the green image possessed a peak due to saturation of the camera pixels by the highly fluorescent GFP-HeLa, indicating and optimal exposure time of 182 ± 7 ms.

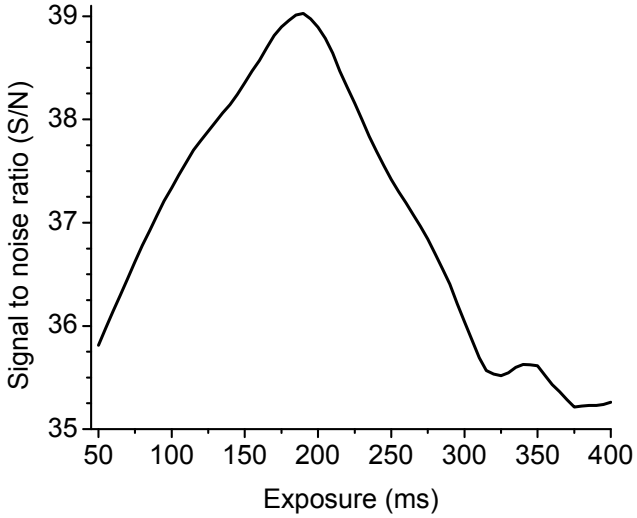


**Figure S2.** Image processing. Signal to noise ratio (S/N) from images of micropallet arrays (n = 4) vs exposure time for the green image.

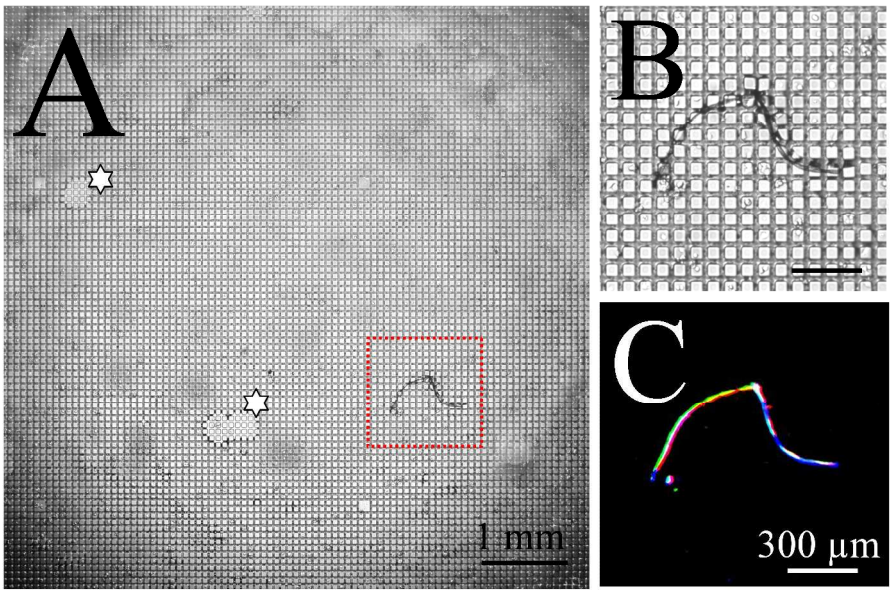


**Figure S3**. (A-B) Brightfield image of a region of a micropallet array showing the presence of a piece of dust. (C) Magnified fluorescence image composite highlighting the light scatter generated by the same debris particle for the green, blue and red images. The 'star' highlights regions of virtual air wall decomposition on the micropallet arrays.

*Background subtraction.* Various methods were screened for their ability to distinguish micropallet autofluorescence and scattering objects (bubbles or debris) from fluorescent cells (Table S2). Five different filtering strategies were tested to increase the S/N for the green image: adaptive wiener filtering, top hat filtering, modified top hat filtering and a combination of adaptive wiener filtering with top hat filtering or modified top hat filtering.[3,9] The top hat filter built into MATLAB was implimented with a disk-shaped structuring element (50 µm diameter). The modified top hat filter first applied a morphological closing (square structuring element of 75 × 75 µm) to eliminate the dark gaps between micropallets, which was followed by a morphological opening (disk structuring element 50 um in diameter) to approximate the image background. Subsequently, this background image was subtracted from the original image.

Background subtraction strategies were evaluated for their ability to generate the greatest S/N as defined above. The background subtraction strategy that provided the greatest increase in the S/N was the modified morphological top hat filter without adaptive noise filtering, 77 ± 7 S/N. Filtering of background signals, as depicted in Figure S4, greatly reduced the micropallet autofluorescence signal intensity, affording better discrimination between fluorescence cells and background during image analysis. Along with improving the S/N, background subtraction also corrected for any uneven illumination in the epi-fluorescent system.

| | Signal (RFU) | Noise (RFU) | S/N (RFU) |
|---|---|---|---|
| Raw Image | 6023 ± 100 | 152 ± 13 | 40 ± 3 |
| Adaptive Wiener Filter | 6009 ± 101 | 147 ± 13 | 41 ± 4 |
| Top-Hat Filter | 5275 ± 97 | 118 ± 12 | 45 ± 5 |
| Adaptive Wiener Filter | 5212 ± 99 | 110 ± 13 | 47 ± 6 |
| + Top-Hat Filter | | | |
| Modified Top-Hat Filter | 4972 ± 72 | 65 ± 6 | 77 ± 7 |
| Adaptive Wiener Filter | 5000 ± 74 | 69 ± 6 | 72 ± 6 |
| + Modified Top-Hat Filter | | | |
| *Signal is mean intensity of objects of interest, n = 4 images, image size 11.7 $mm^2$ | | | |
| *Noise is the standard deviation of the image excluding the objects of interest | | | |
| RFU = arbitrary fluorescence units | | | |

**Table S2**: Background subtraction algorithms

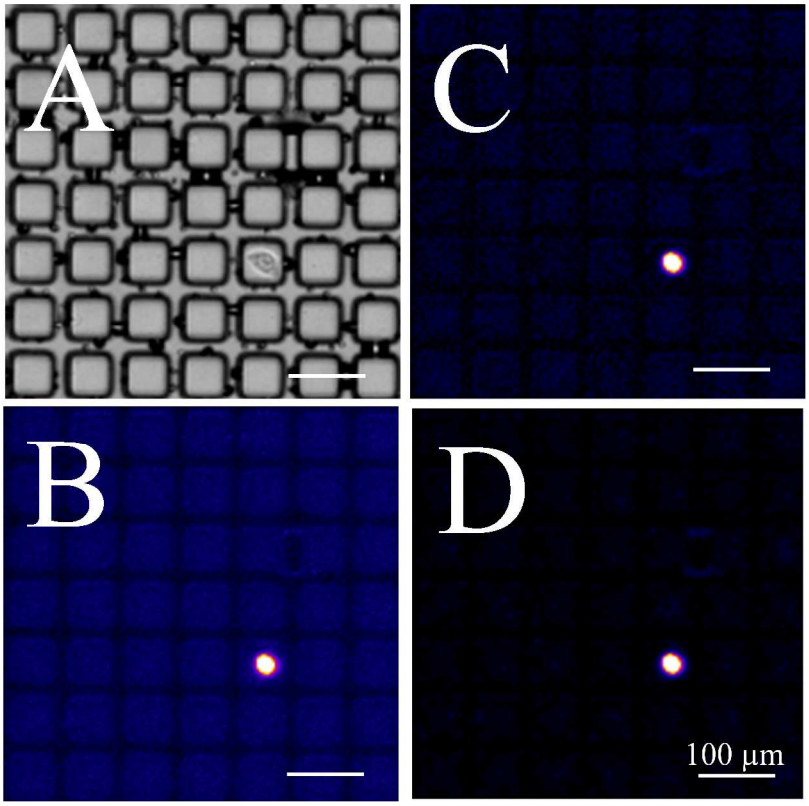


**Figure S4.** Image processing. (A-D) images of a GFP-HeLa cell on an array of micropallets. (A) Brightfield image. (B) Pseudocolor fluorescence image of the raw image acquired using a fluorescein filter set to collect a green image. (C-D) The same image as in panel B but with background subtraction using adaptive wiener filtering (C) or modified top hat filtering (D).

**Image analysis.**

*Image thresholding.* Sensitivity for objects detected using the green filter set was defined as the percentage of GFP-HeLa cells that were successfully identified following image processing and analysis. Initially, the fluorescence intensity threshold (minimum pixel intensity cutoffs) was established to remove low intensity fluorescence signals generated by micropallet autofluorescence and weakly scattering artifacts that remained after image processing. Threshold values ranging from 0 to 10000 were sequentially assessed in increments of 10, and the largest

threshold value that maintained 100% sensitivity, *i.e.* 0% false negatives, was selected as the ideal threshold (Figure S5). An optimal threshold value of 2018 ± 174 was identified for the green image (Table S3). This optimal threshold identified 100% true positives and 0% false negatives while reporting only 5 ± 2 false positives.

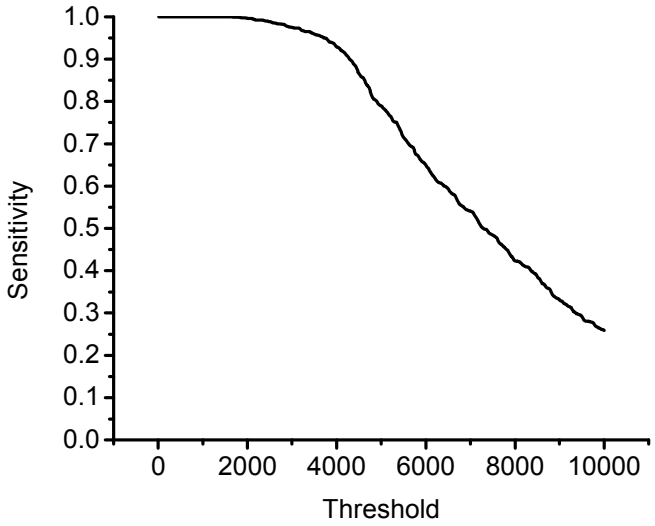


**Figure S5**. The fraction of true positive objects identified vs the threshold.

*Automated thresholding.* Algorithms to automatically select the fluorescence threshold were examined as alternatives to manually selecting a threshold value. These calculations work by various means, with the final goal of differentiating from the fluorescence signal from the background noise. Six different thresholding algorithms were compared to the optimal threshold identified manually. Thresholding algorithms employed were K-Means clustering, K-Means clustering [ignore black], Histogram Trough, Kapur Entropy, Kapur Entropy [ignore black], Mean, Mean [ignore black], Yen Entropy, Yen Entropy [ignore black], Li Entropy and Li Entropy [ignore black].[10] Ignoring black during image thresholding disregards pixel values of zero during threshold calculation. The automated thresholding algorithms were evaluated for their success in

picking a threshold that reported 100% of the true positives while minimizing the generation of false positives (Table S3). Selection of an automated thresholding method was determined by, in order: 1. true positives in the green image, 2. number of false positives in the green image and 3. threshold value proximity to optimal threshold. Following these criteria, the 'Kapur Entropy' thresholding algorithm was selected because it retained 100% true positives while maintaining minimal false positives and was used to give a first-guess threshold value.[11] The 'Li Entropy [ignore black]' algorithm was employed as an upper threshold limit due to the fact that it consistently provided threshold values close to the optimal threshold, but not always with 100% sensitivity.[12] Using the first-guess threshold value and upper threshold value supplied by the 'Kapur Entropy' and 'Li Entropy [ignore black]' algorithms, respectively, the threshold value can be further optimized manually at any point to reduce false positives.

| Filter Set | 159 ± 47 Positive cells | | |
|---|---|---|---|
| Threshold Method | Threshold (RFU) | Sensitivity | False Positives |
| Optimal | 2018 ± 174 | 1.000 ± 0.000 | 5 ± 2 |
| K-Means Clustering | 3130 ± 37 | 0.973 ± 1.012 | 2 ± 1 |
| K-Means Clustering* | 3853 ± 77 | 0.939 ± 0.013 | 1 ± 1 |
| Histogram Trough | 619 ± 113 | 1.000 ± 0.000 | 13 ± 5 |
| Kapur Entropy | 633 ± 47 | 1.000 ± 0.000 | 13 ± 4 |
| Kapur Entropy* | 3538 ± 308 | 0.952 ± 0.021 | 2 ± 1 |
| Mean | 40 ± 7 | 1.000 ± 0.000 | 603 ± 172 |
| Mean* | 1850 ± 136 | 0.996 ± 0.003 | 5 ± 2 |
| Yen Entropy | 728 ± 16 | 1.000 ± 0.000 | 12 ± 4 |
| Yen Entropy* | 2535 ± 318 | 0.979 ± 0.014 | 4 ± 2 |
| Li Entropy | 483 ± 15 | 1.000 ± 0.000 | 14 ± 4 |
| Li Entropy* | 1795 ± 78 | 0.997 ± 0.001 | 6 ± 2 |
| *Ignore 0 value pixels, n = 4 images, image size 11.7 $mm^2$ | | | |
| RFU = arbitrary fluorescence units | | | |

**Table S3**: Automated thresholding algorithms

*Limit of detection.* The sensitivity of the optimized MATLAB program was tested with the implementation of 'Kapur Entropy' automated threshold algorithm. Microspheres (7-9 μm diameter) labeled with fluorescein ranging from 9,828 to 756,101 molecules of equivalent soluble fluorochrome (MESF) units were used to assess the limit of detection of fluorescein for the system. The limit of detection was determined to be between 47,640 and 188,487 MESF units, which permitted successful detection of fluorescein-labeled anti-CD44 on the surface of a cancer stem cell as described in the manuscript. (Table S4).

| Intensity (MESF units) | Sensitivity (%) |
|---:|---:|
| 9828 | 0.454 ± 0.081 |
| 47640 | 0.948 ± 0.019 |
| 188487 | 1.000 ± 0.000 |
| 756101 | 1.000 ± 0.000 |

Table S4. Sensitivity of imaging system for the detection of fluorescein. Images were taken with 1X objective and 2X magnification at 182 ms exposure.

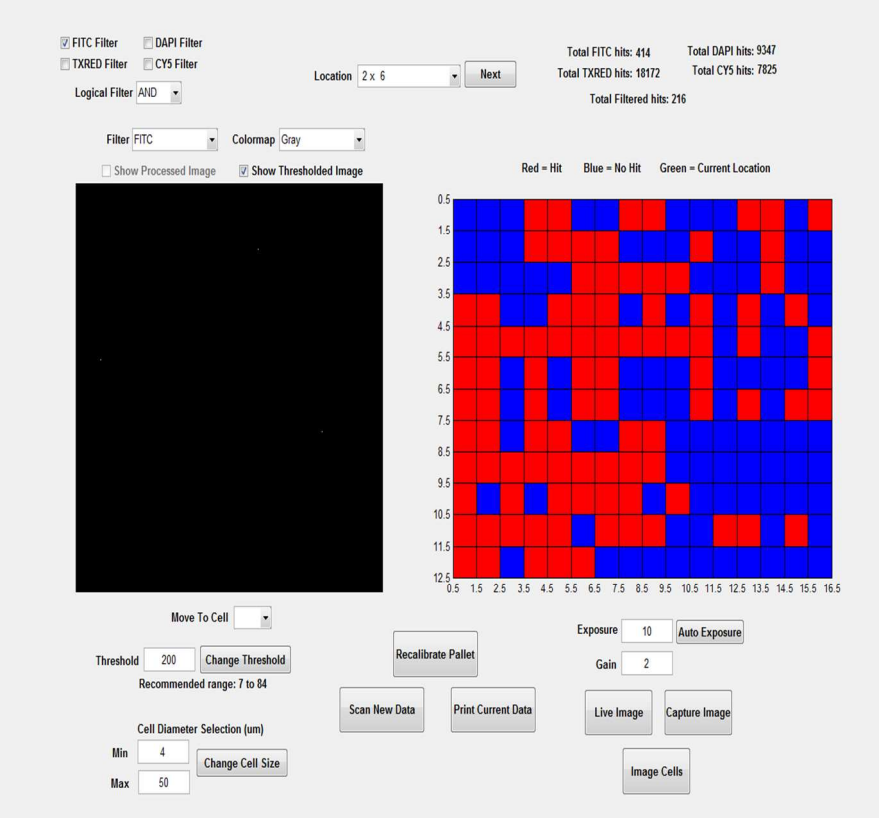


**Figure S6**. Image analysis GUI. Representative image analysis GUI for identifying target cells on the micropallet array. The AnalyzeArray GUI was designed to easily control MATLAB operations for choosing which image wavelength to employ, threshold determination and size-based filtering range. The checkerboard image on the right showed image coordinates where red squares contain 'hits' and blue squares contain no positive objects. The largely black image on the left shows the thresholded image for a specified array location. Also included are numbers for the total object numbers found following thresholding and a command for real-time viewing of select objects.

**REFERENCES**


(1) Gach, P.; Sims, C.; Allbritton, N. *Biomaterials* **2010**, *31*, 8810.

(2) Wang, Y.; Sims, C.; Marc, P.; Bachman, M.; Li, G.; Allbritton, N. *Langmuir* **2006**, *22*, 8257.

(3) Russ, J. C. *The Image Processing Handbook, 6th ed.*; CRC Press, 2011.

(4) Quinto-Su, P. A.; To'a Salazar, G.; Sims, C. E.; Allbritton, N. L.; Venugopalan, V. *Anal. Chem.* **2008**, *80*, 4675.

(5) Wang, Y.; Young, G.; Bachman, M.; Sims, C.; Li, G.; Allbritton, N. *Anal. Chem.* **2007**, *79*, 2359.

(6) Freshney, R. I.; John Wiley & Sons, Inc.: 2010.

(7) Song, L.; van Gijlswijk, R. P.; Young, I. T.; Tanke, H. J. *Cytometry* **1997**, *27*, 213.

(8) Stephens, D. J.; Allan, V. J. *Science* **2003**, *300*, 82.

(9) Martin, D.; Sandoval, S.; Ta, C.; Ruidiaz, M.; Cortes-Mateos, M.; Messmer, D.; Kummel, A.; Blair, S.; Wang-Rodriguez, J. *Acta Cytol.* **2011**, *55*, 271.

(10) Sezgin, M.; Sankur, B. *J. Electron. Imaging* **2004**, *13*, 146.

(11) Kapur, J.; Sahoo, P.; Wong, A. *Comput. Gr. Image Process.* **1985**, *29*, 273.

(12) Li, C.; Tam, P. *Pattern Recogn. Lett.* **1998**, *19*, 771.